Nagel, Erick; D'Alessio, Paola; Calvet, Nuria; Espaillat, Catherine; Angel Trinidad, Miguel
THE EFFECT OF SUBLIMATION TEMPERATURE DEPENDENCIES ON DISK WALLS AROUND T
TAURI STARS

THE EFFECT OF SUBLIMATION TEMPERATURE DEPENDENCIES ON DISK WALLS AROUND T TAURI STARS

Erick Nagel,[1] Paola D'Alessio,[2] Nuria Calvet,[3] Catherine Espaillat,[4] and Miguel Angel Trinidad[1]

RESUMEN

El polvo no puede sobrevivir más cerca de la estrella de un punto donde alcanza una temperatura igual a la temperatura de sublimación. La frontera entre una región sin polvo y polvosa define la pared de sublimación. En la literatura se usan dos modelos para la estructura de la pared: una pared con temperatura de sublimación fija y una con temperatura de sublimación dependiente de la densidad. En la primera, la pared es vertical y en la segunda, la pared es curva. Encontramos diferencias importantes entre las SEDs de estos modelos en el intervalo de longitudes de onda desde 3 a 8 μm, siendo la emisión de la primera más grande que la segunda. Cuantificamos las diferencias en los colores de IRAC cuando se usan estos modelos para explicar las observaciones. En el diagrama de IRAC color-color ([3.6]–[4.5] vs. [5.8]–[8.0]), los modelos están localizados en regiones específicas, dada la inclinación, la tasa de acreción de masa, o el modelo usado.

ABSTRACT

The dust cannot survive closer to the star from the point where a grain reaches a temperature equal to the sublimation temperature. The boundary between a dust-free and a dusty region defines the sublimation wall. In the literature two models for the structure of the wall are used: a wall with a fixed sublimation temperature and a wall with a density-dependent sublimation temperature. In the former case, the wall is vertical and in the latter, the wall is curved. We find important differences between these models' SEDs in the wavelength range from 3 to 8 μm, the emission of the former being larger than that of the latter model. We quantify the differences in IRAC colors when these models are used to explain the observations. In the IRAC color-color diagram ([3.6]–[4.5] vs. [5.8]–[8.0]), the models are located in specific regions, either depending on the inclination, the mass accretion rate, or the model used.

Key Words: infrared: general — protoplanetary disks — stars: pre-main sequence

1. INTRODUCTION

One of the motivations for the study of the dust in the protoplanetary disks inner regions is the fact that terrestrial planets are formed there (Goldreich & Ward 1973; Alibert et al. 2010). The dust might not survive if the dust grains reach temperatures higher than the sublimation temperature. Thus, the innermost region of a disk around a star is dust free and has an opacity hole or deficit. The outer boundary of the hole formed in this way is called a sublimation wall or the disk inner rim. This surface separates an outer dusty and an inner gaseous disks, and its shape depends on the characteristics of the gas and the dust.

Hillenbrand et al. (1992) model the near-infrared (NIR) excess of Herbig Ae/Be stars as coming from material located at the inner rim of the disk with a temperature around 1500 K. This is consistent with the evaporation temperature of silicate grains. Thus, they conclude that the emission is produced in a sublimation wall. In fact, the edge of the hole produced by dust sublimation mostly emits in the

---

[1]Departamento de Astronomía, Universidad de Guanajuato, Guanajuato, Mexico.

[2]Centro de Radioastronomía y Astrofísica, Universidad Nacional Autónoma de México, Morelia, Michoacán, Mexico.

[3]Department of Astronomy, University of Michigan, USA.

[4]Harvard-Smithsonian Center for Astrophysics, USA.

NIR. The modeling of the NIR excesses as produced in this kind of walls has been pursued by many workers (Tuthill, Monnier, & Danchi 2001; Eisner et al. 2005; Akeson et al. 2005; Monnier et al. 2005; Millan-Gabet et al. 2007). A nice characterization of the shape of the wall using a Monte Carlo radiative transfer code, taking into account stratification of grains was developed by Whitney et al. (2004). They found an empirical formula for the radius of the sublimation wall ($R_{\rm wall}$) in terms of the evaporation temperature $T_{\rm sub}$ ($R_{\rm wall} \propto T_{\rm sub}^{-2.085}$), which is consistent with simplified expressions commonly used. The range of dust sublimation temperature in terms of gas density is between 10^{-18} and 10^{-4} g cm^{-3} and it is given for different grain species by Pollack et al. (1994). For silicate olivine, the range is (929–1774) K; for silicate pyroxene, $T_{\rm sub} = (920-1621)$ K; for troilite, $T_{\rm sub} = 680$ K; and for iron the range is (835–1908) K.

For the case of very low luminosity systems as the brown dwarfs, Mayne & Harries (2010) note that the location of the dust sublimation wall is equal to the disk co-rotation radius with the magnetosphere, as was also suggested by Eisner et al. (2007). For this case and also for configurations where the sublimation wall is inside the co-rotation radius, the magnetic field truncates the disk. Thus, the resulting shape of the wall depends strongly on this processes and weakly on the sublimation phenomenon. In our case, the stellar luminosity is large enough to move the wall outside the magnetosphere. Thus, its geometry is given by the physical state of dust and gas.

Taking a unique sublimation temperature leads to a unique radius, hence to a vertical wall. We refer to this model as $T_{0,\rm fix}$ wall. For this model, we use a sublimation temperature characteristic of the disk midplane, and assume it is the same at every height (in spite of the variation of density with height). This implies that the wall is vertical, i.e., the inner surface of a hollow cylinder, but also that the surface temperature is constant (and equal to the assumed sublimation temperature). On the other hand, if we take into account the dependence of the sublimation temperature with density, the wall is curved. We refer to this model as $T_{0,\rho}$ wall. The variation of density with height and radius in disk models is taken from structures assumed to be in vertical hydrostatic equilibrium. Again, there is a twofold effect, affecting the solid angle of the visible portions of the wall, and also the surface temperature of the wall, which is different at each pixel. When we compare the SED of a $T_{0,\rm fix}$ wall with that of a $T_{0,\rho}$ wall, both effects are present, i.e., differences in area and in temperature, but they are difficult to disentangle.

If the gas density and the dust composition do not depend on the vertical coordinate, then a $T_{0,\rm fix}$ wall is formed. We want to point out the fact that sometimes due to the unknowns of the composition and density profile, one is naturally led to simplify the system and assume a homogeneous vertical distribution of matter. However, as we will see in the following, a vertical stratified model curves the wall. Previously, the assumption was that the shape of the wall was vertical (Dullemond, Dominik, & Natta 2001; D'Alessio et al. 2005). However, for the modeling of the stationary state of the disk around EX Lup (Sipos et al. 2009), a $T_{0,\rm fix}$ wall was unable to explain the IR observations, and an *ad hoc* rounded inner rim was required. A non-vertical wall was also considered by Isella & Natta (2005); they interpreted a 2 μm emission bump, in observed SEDs of Herbig Ae stars, as coming from a sublimation wall. They considered that due to the density dependence on the sublimation temperature the wall was curved. Two years later Tannirkulam, Harries, & Monnier (2007) pursued this further, taking into account grain sedimentation. The dust is composed of two grain size distributions, characterized by different scale heights. In these works a $T_{0,\rho}$ wall model can reproduce the Herbig Ae stars NIR spectrum. Isella & Natta (2005) and Tannirkulam et al. (2007) studied the differences between synthetic images of $T_{0,\rm fix}$ and $T_{0,\rho}$ wall models; here, we analyse the effects on the colors. Unfortunately the spatial resolution and limited sensitivity, and the small number of telescopes for NIR interferometric observations, make it difficult to confirm the geometry of the inner region (Dullemond & Monnier 2010). Thus, we have some intrinsic degeneracy on the models used to interpret the data. Due to this, it is important to include all the physics that we can on the models of these walls.

In this work, we consider that sublimation is the mechanism responsible to produce the inner hole; the physics involved in this process shapes the wall. Note that a recently formed planet (Quillen et al. 2004) and a photodissociation flux (Clarke, Gendrin, & Sotomayor 2001) are also able to create a hole. The magnetic rotational instability is responsible for creating a wind, which in turn is able to form a hole (Suzuki, Muto, & Inutsuka 2010). A binary system is another way to create a hole, in this case by gravitational interactions (Hartmann et al. 2005a; Espaillat et al. 2007; Nagel et al. 2010). The physical pecu-

TABLE 1

MAXIMUM T_{WALL} AND MINIMUM R_{WALL}

Model	min(R_{wall}) (AU)	max(T_{wall}) (K)
$T_{0,\mathrm{fix}}$ ($\dot{M} = 1.625 \times 10^{-8}\ M_\odot\ \mathrm{yr}^{-1}$)	0.0715	1400
$T_{0,\mathrm{fix}}$ ($\dot{M} = 3.25 \times 10^{-8}\ M_\odot\ \mathrm{yr}^{-1}$)	0.079	1400
$T_{0,\mathrm{fix}}$ ($\dot{M} = 6.5 \times 10^{-8}\ M_\odot\ \mathrm{yr}^{-1}$)	0.0915	1400
$T_{0,\rho}$ ($\dot{M} = 1.625 \times 10^{-8}\ M_\odot\ \mathrm{yr}^{-1}$)	0.0802	1402
$T_{0,\rho}$ ($\dot{M} = 3.25 \times 10^{-8}\ M_\odot\ \mathrm{yr}^{-1}$)	0.0801	1453
$T_{0,\rho}$ ($\dot{M} = 6.5 \times 10^{-8}\ M_\odot\ \mathrm{yr}^{-1}$)	0.0971	1430
Eisner et al. (2009)		
RY Tau	0.16	1750
DG Tau	0.18	1260
RW Aur	0.14	1330
AS 205A	0.14	1850

liarities of each process will define the structure for the wall.

In a sense, this work follows the steps of Isella & Natta (2005), because we are taking into account the same physics to describe the grain sublimation. However, one difference is that we focus on T Tauri instead of Herbig Ae stars. Our first aim is to compare models of $T_{0,\rho}$ and $T_{0,\mathrm{fix}}$ walls, characterizing parameters like location and surface temperature. Other questions to address are: if we change the inclination or the mass accretion rate, is it still possible to discriminate between a $T_{0,\mathrm{fix}}$ and a $T_{0,\rho}$ wall based only on the SED? Based on the Infrared Array Camera (IRAC, on board the *Spitzer Space Telescope*) observations, does a model of a disk plus a $T_{0,\mathrm{fix}}$ wall or a disk plus a $T_{0,\rho}$ wall show differences in the IRAC colors? It is noteworthy that Isella & Natta (2005) mention that based on an image is easy to discriminate between models, because for the $T_{0,\mathrm{fix}}$ one, only the half of the wall that is farthest from the observer will show emission in the line of sight. The observed $T_{0,\rho}$ wall emission comes from every azimuthal angle of the wall. Without an image, one cannot choose between both models. However, looking at the differences in the SED is a way to argue whether for the problem at hand it is enough to take a $T_{0,\mathrm{fix}}$ model.

The minimum location of the wall (where the maximum temperature occurs) is a parameter that changes when using $T_{0,\mathrm{fix}}$ or $T_{0,\rho}$ wall models. One can conclude in the following sections that this parameter differs at most by 10% (see Table 1). In the case of the IRAC colors, between the $T_{0,\rho}$ and $T_{0,\mathrm{fix}}$ wall models, the [3.6]–[4.5] and [5.8]–[8.0] col-

ors changes around 20% and 10%, respectively. In § 2 we present the details of the code used in this work, followed in § 3 by the resulting characteristics of the walls, either the $T_{0,\mathrm{fix}}$ (§ 3.1) or the $T_{0,\rho}$ (§ 3.2). § 4 shows the IRAC colors associated to the models presented. Finally, in § 5 we present a summary and the conclusions.

2. DESCRIPTION OF THE CODE

The $T_{0,\mathrm{fix}}$ wall emission is calculated with the code used in D'Alessio et al. (2005) for an isolated star or for a binary system in Nagel et al. (2010). We consider that the wall is optically thick but the emission from an optically thin atmosphere is taken into account. The wall is heated by the impinging geometrically diluted stellar radiation flux coming from the photosphere of the star and from the accretion shocks. We assume that the stellar radiation is plane parallel. Thus, for a $T_{0,\mathrm{fix}}$ wall, the radiation arriving at each point is the same. The total emission is the addition of the contribution of each layer at given τ, extinguished by the material in front of it. The temperature is calculated following Calvet et al. (1991) and D'Alessio et al. (2005).

We have assumed that the opacities are independent of τ, in accordance with Calvet et al. (1991), Calvet et al. (1992) and D'Alessio et al. (2005). This is a necessary assumption in order to find an analytical expression for $T(\tau)$. The temperature at every depth of the wall atmosphere is lower than the sublimation temperature. Thus, there is no sublimation of dust, and it is safe to take a constant opacity.

The geometrical effects producing shadowing of regions of the wall by regions of the wall closer to

the observer are taken into account. The SED of the wall is calculated integrating the flux of every point in the wall whose normal has a component in the direction of the observer, multiplied by the solid angle subtended by every pixel.

The minimum ($a_{\min}$) and maximum size ($a_{\max}$) of the grains is 0.005 μm and 0.25 μm, respectively; the power law exponent is -3.5; these are parameters typical for interstellar grains (Mathis, Rumpl, & Nordsieck 1977). The dust is composed of silicates (pyroxenes, $Mg_{0.8} Fe_{0.2} SiO_3$; and olivines, $Mg Fe SiO_4$), graphite and troilite. We adopt a dust-to-gas mass ratio for the silicates, $\zeta_{\mathrm{sil}} = 0.0034$ (Draine & Lee 1984); for the graphite, $\zeta_{\mathrm{grap}} = 0.0025$; and for the troilite, $\zeta_{\mathrm{troi}} = 7.68 \times 10^{-4}$. The composition and abundance are typical for accretion disks (Pollack et al. 1994). The optical properties of the silicates come from Dorschner et al. (1995). For the dust composition chosen, the silicates are the grains with the highest sublimation temperature. From this follows the fact that the silicates rule the location and shape of the wall. Dust species with a higher sublimation temperature as corundum (Al_2O_3), in principle will affect the location and structure of the wall, because such grains are the ones formed closest to the star (Verhoelst et al. 2006). A consistent modeling of a disk with corundum requires a study that at the same time takes into account the gas and dust opacity, because in the temperature range where corundum is formed, the gas contribution to the opacity is a sizable fraction of the total opacity. In the region where the silicates grains are formed, the silicates opacity is around 6 orders of magnitude larger than the gas opacity (Ferguson et al. 2005). Thus, it is not necessary to include the gas contribution in the case treated here. This is the reason why in the sublimation wall formation is not important to know the gas opacity, something that we cannot leave aside when corundum is included in the mixture.

A near-IR emission study of a disk-star system should include the contribution of a gaseous disk inside the sublimation wall. The importance of this is highlighted in the interpretation of interferometric observations by Tannirkulam et al. (2008) and Eisner et al. (2010). Either for the study of the dust-free gaseous disk emission or the shaping of the wall by the presence of corundum, a detailed knowledge of the gas opacity is necessary. This is a non trivial issue, because of the presence of millions of lines and also, because it is not clear what kind of mean opacity is representative for the approach used here. Due to this, the gas emission problem is beyond the scope of this paper, but should be taken into account in the future.

The $T_{0,\rho}$ wall emission is calculated based on the code just described, but including an arbitrary shape for the wall. Unlike a $T_{0,fix}$ wall, for the $T_{0,\rho}$ wall, the radiation arriving at different places of the wall is not the same. The impinging flux depends on the angle of incidence α, (the angle between the normal to the wall surface and the incidence ray); specifically it is proportional to $\cos\alpha$, which in turn depends on the wall shape. Thus, we have to characterize α in order to get a value for the temperature in the wall. In other words, we need to know beforehand α to get the temperature, but we require the temperature to calculate α, that is, the wall shape. A way to solve this problem is to note that if the scattering of the stellar radiation is neglected along with the heating from inner regions (viscously produced), an expression for $T(\tau = 0)$ without dependence on α is found. The contribution of the scattered emission has the characteristic frequency range of the stellar radiation. Thus, its main contribution is at wavelengths smaller than the peak of the emission of sublimation walls. Because of this, it is reasonable to neglect the scattering when one focusses on the infrared frequency range. Using this expression, the wall shape is defined by the points where this temperature is equal to the sublimation temperature. This results in a shape for the wall surface from which an incidence angle can be calculated. With these assumptions, the temperature as a function of τ can be written as:

$$T(\tau)^4 = \frac{(L_\star + L_{\mathrm{acc}})\cos\alpha}{16\sigma\pi r^2}(c_1 + c_2 e^{-\frac{q\tau}{\cos\alpha}}), \quad (1)$$

where $q = \kappa_{\mathrm{inc}}/\kappa_d$,

$$c_1 = \frac{3\cos\alpha}{q}, \quad (2)$$

and

$$c_2 = \frac{q}{\cos\alpha} - \frac{3\cos\alpha}{q}. \quad (3)$$

Then, the temperature at the surface ($\tau = 0$) is

$$T(\tau)^4 = \frac{(L_\star + L_{\mathrm{acc}})\cos\alpha}{16\sigma\pi r^2}\left[\frac{3\cos\alpha}{q} + \left(\frac{q}{\cos\alpha} - \frac{3\cos\alpha}{q}\right)e^{-\frac{q\tau}{\cos\alpha}}\right], \quad (4)$$

and we know that it should be equal to the sublimation temperature, $T_{\mathrm{sub}}(\rho(z,R))$ (Pollack et al. 1994), which depends on the density. This results in an equation for $\alpha(z,R)$. Here, κ_{inc} and κ_d are

the mean opacity of true absorption, evaluated at the temperature characteristic of the incident stellar radiation, and at the temperature of the disk, respectively, $L_\star$ is the luminosity of the star and $L_{\rm acc}$ is the luminosity produced by the shocks of the material accreting along the magnetic field lines. Note that q depends on the temperature, thus equation 4 is solved iteratively. Knowing the temperature, the radius of dust destruction is calculated substituting $\tau = 0$ in equation 4, thus,

$$r_{\rm des}(z)^2 = \frac{L_\star + L_{\rm acc}}{16\pi\sigma}\left(\frac{\kappa_{\rm inc}}{\kappa_d}\right)\frac{1}{T_{\rm sub}(z)^4}, \qquad (5)$$

in which the scattering and the local radiation field are neglected.

3. CHARACTERISTICS OF WALLS

The differences in the SED when comparing a $T_{0,\rho}$ and a $T_{0,\rm fix}$ wall are the result of a combination of, at least, two effects: (1) geometry, because in a $T_{0,\rho}$ wall, each pixel shows a different effective area to the observer than in a $T_{0,\rm fix}$ wall, and (2) surface temperature gradient, because what we are assuming that curves the wall is the dependence of the sublimation temperature on density. This implies that at each height, the surface of the wall would have a different temperature than a $T_{0,\rm fix}$ wall, defined by a unique sublimation temperature.

In this section we calculate the wall emission using the code described in § 2. Our intention is to construct models for the wall emission for a typical young low-mass star: $M_\star = 0.5\ M_\odot$, $R_\star = 2.0\ R_\odot$, $T_\star = 4000$ K, and $\dot{M} = 3.25 \times 10^{-8}\ M_\odot\ {\rm yr}^{-1}$ (Gullbring et al. 1998). This is our fiducial system. Two kinds of models are considered. The first one is a $T_{0,\rm fix}$ wall with constant surface temperature, the second is a wall with a shape given by how the sublimation temperature depends on density (see Figure 1).

As noted in § 1, the modeling of interferometric observations primarily depends on two basic parameters: a typical distance to the emission region, and a typical temperature. In order to compare these parameters with other works, we present in Table 1 for all the models, either the $T_{0,\rm fix}$ or the $T_{0,\rho}$ walls; the values of the minimum radius of the wall and the temperature at this location. For comparison, in Table 1 the parameters for the models of the four T Tauri stars presented in Eisner et al. (2009) are shown. We do not expect a concordance between the values, but rather the opposite, because this set of values comes from two different approaches. Our modeling produces these values from
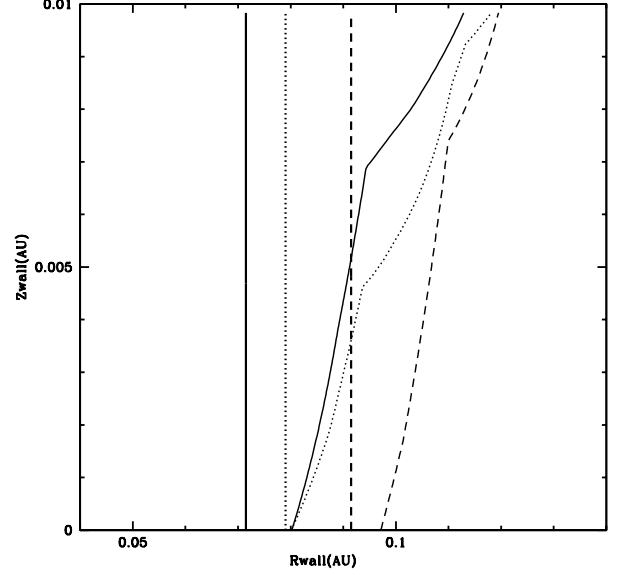

Fig. 1. The shapes of the $T_{0,\rm fix}$ walls are shown as thin lines. The $T_{0,\rho}$ walls shapes are presented as thick lines. Models presented have $\dot{M} = 1.625 \times 10^{-8}\ M_\odot\ {\rm yr}^{-1}$ (solid line), $\dot{M} = 3.25 \times 10^{-8}\ M_\odot\ {\rm yr}^{-1}$ (dotted line), and $\dot{M} = 6.5 \times 10^{-8}\ M_\odot\ {\rm yr}^{-1}$ (dashed line).

a detailed description of the wall formation. Eisner et al. (2009) interpret their interferometric observations with $R_{\rm wall}$ and $T_{\rm wall}$ as two free parameters of a simplistic model. In their model these parameters are fitted without a model of the star or dust composition.

An important fact to notice here is that to obtain the interferometric image of the infrared observational data a prior knowledge of the observed structure is required. Then the physical parameters extracted from infrared interferometric observations are calculated using a particular model; in other words, they are model dependent. These difficulties are not present in radio interferometry, where the large number of points in the visibility plane, along with the high angular resolution and sensitivity obtained, allows the application of the inverse Fourier transformation to get a real image of the object, that does not depend on a particular model. In the case of NIR interferometry, the number of visibilities is so low that we cannot invert the problem. Thus, we depend on a model to extract the parameters of the system.

Summarizing, we should be careful to compare the set of parameters extracted in this way with values given by a model independent of observations. Eisner et al. (2004) uses five different models to interpret the interferometric observations of 14 Herbig
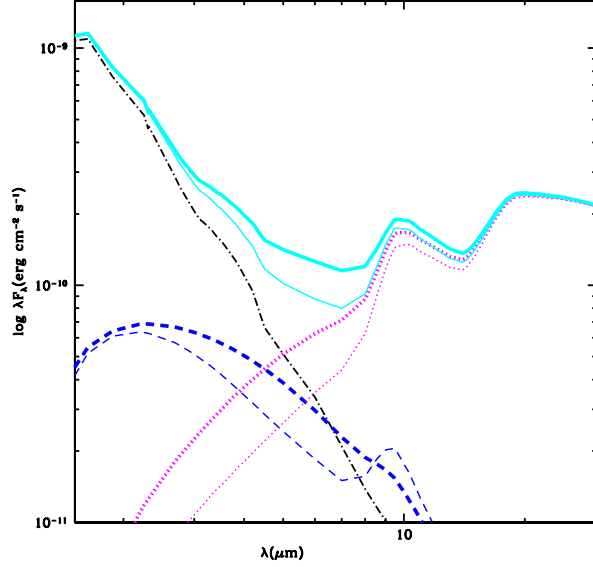
Fig. 2. SEDs for the $T_{0,\text{fix}}$ model (thick line), and for the $T_{0,\rho}$ wall shaped by the dependence of the sublimation temperature on density (thin line) for the fiducial model. The dashed lines represent the wall spectrum, the dotted lines the disk SED and the solid lines the total emission. The disk inclination is $\cos i = 0.5$. The color figure can be viewed online.
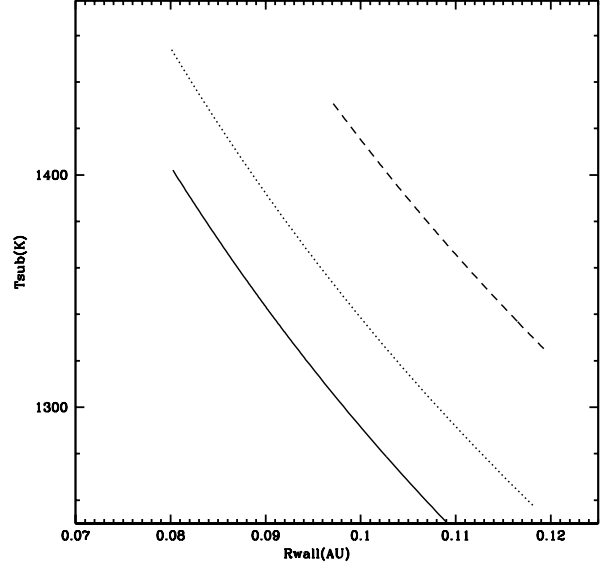

Fig. 3. The sublimation temperature T_{sub} along the $T_{0,\rho}$ wall surface is shown as a solid line for $\dot{M} = 1.625 \times 10^{-8}$ $M_\odot$ yr^{-1}, as a dotted line for $\dot{M} = 3.25 \times 10^{-8}$ $M_\odot$ yr^{-1}, and as a dashed line for $\dot{M} = 6.5 \times 10^{-8}$ $M_\odot$ yr^{-1}.

Ae/Be stars at 2.2 μm. These span geometries such as an envelope, disk or ring. Looking for the best fit allows one to choose the model. However, this do not completely guarantee that the right model is chosen. A qualitative comparison between the models presented here and the model consistent with observations can be done (see Table 1).

For a $T_{0,\rho}$ sublimation wall model we note that the sublimation temperature (T_{sub}) depends on the density (Pollack et al. 1994). Since the density decreases with height and T_{sub} increases with density, the modeled shape is convex. The lower denser parts of the wall are closer to the star; at high altitudes the density decreases, T_{sub} decreases and the wall moves further out. The density structure is given by a disk modeled with a detailed 2D numerical solution of the radiation transfer equations (D'Alessio et al. 1998). Models built with this assumption were previously given by Isella & Natta (2005) for Herbig Ae stars.

3.1. $T_{0,\text{fix}}$ WALL

A $T_{0,\text{fix}}$ wall is defined by a constant sublimation temperature at its surface; here we take $T_{\text{sub}} = 1400$ K. For the luminosity of the typical low-mass star, the sublimation radius (equal to the wall location) is $R_{\text{sub}} = 0.079$ AU. The height of the wall

is taken as 5 times the pressure scale height (Dullemond et al. 2001). Note that the parameters required to define a $T_{0,\text{fix}}$ wall are T_{sub} (or R_{sub}) and a height (see Figure 1).

The SED of this model is presented in Figure 2. In order to do a fair comparison, we add to the wall and star spectra a model of a disk with an inner radius equal to the location of the wall and an outer radius equal to 100 AU. The disk model is done using D'Alessio et al. (1998). The values of T_{sub} and R_{sub} for this model are presented in Table 1. Note that the wall spectrum does not show the 10 μm silicate spectrum. Models changing the disk inclination and the mass accretion rate are presented in § 3.2.

3.2. $T_{0,\rho}$ WALL

The shape of the $T_{0,\rho}$ wall is given by the fact that T_{sub} depends on density (Pollack et al. 1994). The densest parts close to the midplane have a T_{sub} larger than the T_{sub} of the upper layers of the disk. Thus, the former is closer to the star than the latter. The density vertical profile is taken from 2D axisymmetric disk models (D'Alessio et al. 1998).

Figure 3 presents a plot of T_{sub} vs R_{wall} for this case, which shows a temperature decreasing with radius, as one expects from a disk with a density decreasing with an increasing radius. The shape of the wall is given in Figure 1, either for $T_{0,\rho}$
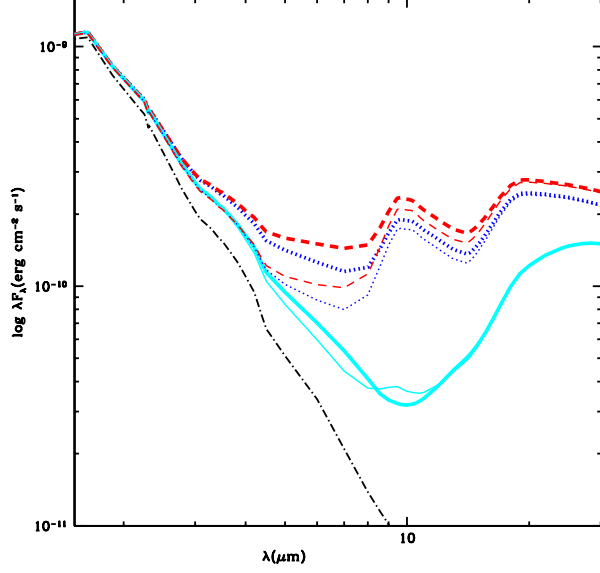
Fig. 4. The spectrum of a $T_{0,\text{fix}}$ model (thick lines), and the $T_{0,\rho}$ model (thin lines). The inclinations shown corresponds to $\cos i = 0.3$ (solid lines), $\cos i = 0.5$ (dotted lines), and $\cos i = 0.7$ (dashed lines). The color figure can be viewed online.
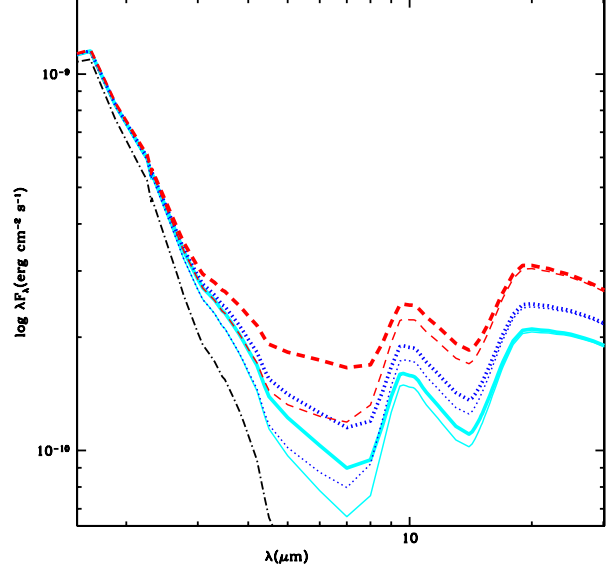

Fig. 5. The spectrum of a $T_{0,\text{fix}}$ model (thick lines), and the $T_{0,\rho}$ model (thin lines) in terms of mass accretion rate. The mass accretion rates shown corresponds to $\dot{M} = 1.625 \times 10^{-8}$ $M_\odot$ yr^{-1} (solid line), $\dot{M} = 3.25 \times 10^{-8}$ $M_\odot$ yr^{-1} (dotted line), and $\dot{M} = 6.5 \times 10^{-8}$ $M_\odot$ yr^{-1} (dashed line). The color figure can be viewed online.

or $T_{0,\text{fix}}$ walls for three values of $\dot{M}$. The value $\dot{M} = 3.25 \times 10^{-8}$ $M_\odot$ yr^{-1} corresponds to the fiducial model; for comparison two models with half and twice this value are presented. Note that the $T_{0,\text{fix}}$ wall location is given at the position where the temperature is equal to 1400 K. The $T_{0,\rho}$ walls are located consistently outwards of the $T_{0,\text{fix}}$ walls.

Figure 2 also presents the spectrum of the fiducial $T_{0,\rho}$ wall model. The model includes the outer disk, starting in this case at the outer radius of the $T_{0,\rho}$ wall. The $T_{0,\text{fix}}$ wall emission is higher than the $T_{0,\rho}$ for $\lambda < 8$ μm. Also, the emission of the disk associated with the $T_{0,\text{fix}}$ wall is higher because in this case the outer disks starts at a smaller radius. Putting these facts together, the SED of a system with a $T_{0,\text{fix}}$ wall is noticeably higher than the model with a $T_{0,\rho}$ wall. This occurs mainly between 3 and 8 μm, resulting in differences between the IRAC colors, as it is described in § 4.

Both the mass accretion rate and the inclination are parameters not well defined or even not defined at all for real systems. In order to display models with different values for these parameters and to be sure that the models do not overlap, we present another set of models. Figure 4 presents for the fiducial model, the behavior of the spectrum with inclination, either for $T_{0,\text{fix}}$ or $T_{0,\rho}$ models. It is important to note that for each type of wall the emission de-

creases as the inclination increases. Note that for a higher inclination, the surface of the disk in the sky plane decreases, which naively means a lower emission. Besides, note that at $\lambda < 8$ μm, a $T_{0,\text{fix}}$ wall model with $\cos i = 0.5$ (60°) emits more than a $T_{0,\rho}$ wall with $\cos i = 0.7$ (45°). It is important to point out that the shape of the SED for these two models is different. Thus, in principle a change in inclination is not able to match models with a $T_{0,\rho}$ and a $T_{0,\text{fix}}$ wall. In this way, a modeler should be able to distinguish between these two scenarios, of course depending on the resolution and precision of the spectrum.

In Figure 5 plots for the SED in terms of $\dot{M}$ are presented. It is expected that either for the $T_{0,\text{fix}}$ or $T_{0,\rho}$ wall models, increasing $\dot{M}$ means a larger flux, and this does not mean just to move the SED by a constant amount, but a change in the shape of the curve. Note that the emission for a $T_{0,\text{fix}}$ wall model with $\dot{M} = 3.25 \times 10^{-8}$ $M_\odot$ yr^{-1} is larger than the emission from a $T_{0,\rho}$ wall model with $\dot{M} = 6.5 \times 10^{-8}$ $M_\odot$ yr^{-1} for $\lambda < 7$ μm. This is an example of the differences between $T_{0,\rho}$ and $T_{0,\text{fix}}$ wall models, which correspond to changes in the IRAC colors as can be seen in § 4.

4. COLOR INDICES

In Allen et al. (2004) there is a comparison of IRAC colors between models with $T_{0,\text{fix}}$ walls and a sample of young stellar objects. Here, we note a difference in the SED between the models with $T_{0,\text{fix}}$ and $T_{0,\rho}$ walls in the wavelength range defined by 3 and 8 μm. This means that the IRAC colors will show variations between the models. The emission of the $T_{0,\text{fix}}$ wall that they use is a blackbody at the typical sublimation temperature of 1400 K. Note that the emission from our model for the $T_{0,\text{fix}}$ wall comes from the atmosphere, with the surface at 1400 K, but the inner parts a little bit cooler. This means that our colors and theirs, for models with the same parameters, should not be the same. The [3.6]–[4.5] color range coincides in Allen et al. (2004) and this work. The [5.8]–[8.0] color value associated to our models is consistently larger than the values in Allen et al. (2004). Note that even for the $T_{0,\text{fix}}$ walls, the emission comes from material with a range of temperatures, in particular, at temperatures lower than 1400 K, which is the temperature taken in Allen et al. (2004). This should change in particular the [5.8]–[8.0] color. The zero point magnitudes are taken as in Hartmann et al. (2005b), consistent with a Vega-based IRAC magnitude system.

Recently, McClure et al. (2010) estimate spectral indices in the range between 6 and 31 μm for disk models, using $T_{0,\text{fix}}$ walls at 1400 K. As noted here, a change in the emission due to a $T_{0,\rho}$ wall instead of a $T_{0,\text{fix}}$ wall will modify the spectral indices. However, due to the dispersion of the values in McClure et al. (2010), including a $T_{0,\rho}$ wall will not change their main conclusions. On the other hand, when one tries to fit specific objects, taking into account a $T_{0,\rho}$ wall should be an unavoidable modeling requirement.

In Figure 6, the IRAC color-color diagram is presented for $T_{0,\text{fix}}$ and $T_{0,\rho}$ wall models. Models with $\dot{M} = (1.625, 3.25, 6.5) \times 10^{-8}$ $M_\odot$ yr^{-1}, and $\cos i = (0.3, 0.5, 0.7)$ are presented. The $\cos i = 0.3$ $T_{0,\text{fix}}$ wall models are clearly located around $[3.6] - [4.5] \sim 0.4$ and $[5.8] - [8.0] \sim 0.65$. The less inclined models move up and to the right in this plot, either for the $T_{0,\text{fix}}$ or $T_{0,\rho}$ walls models. The $T_{0,\rho}$ wall models compared with their $T_{0,\text{fix}}$ counterparts, decrease the [3.6]–[4.5] color and increase the [5.8]–[8.0] color. The trend of the colors in the plot changing $\dot{M}$ and $\cos i$, allows us to confidently say that there is no overlapping of the $T_{0,\rho}$ and $T_{0,\text{fix}}$ wall models. Thus, one cannot confuse a $T_{0,\text{fix}}$ and a $T_{0,\rho}$ wall model when changing these two parameters.

In the last paragraph, we stress that the various models are located in specific regions of the color-
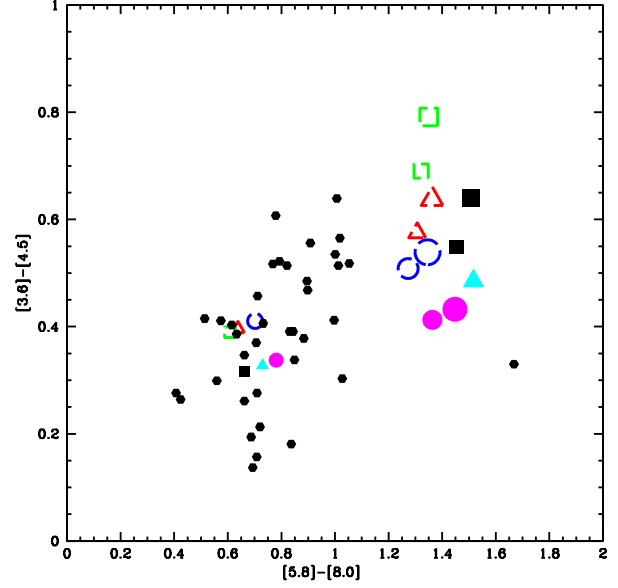

Fig. 6. IRAC colors for models including star, wall and disk. The models with a $T_{0,\text{fix}}$ wall or a $T_{0,\rho}$ wall are presented by open and filled symbols, respectively. Models for the following mass accretion rates are shown: $\dot{M} = 1.625 \times 10^{-8}$ $M_\odot$ yr^{-1} (circles), $\dot{M} = 3.25 \times 10^{-8}$ $M_\odot$ yr^{-1} (triangles), and $\dot{M} = 6.5 \times 10^{-8}$ $M_\odot$ yr^{-1} (squares). The smaller size symbols correspond to an inclination given by $\cos i = 0.3$, the medium size correspond to $\cos i = 0.5$, and the larger size to $\cos i = 0.7$. The black points correspond to the sample of Class II pre-main-sequence objects in Hartmann et al. (2005b). The color figure can be viewed online.

color diagram. Looking at the models in Figure 6, there is no degeneracy with the inclination. At first sight, this seems a surprising result, because it is usually assumed that the inclination can work as a tuning parameter for the emitted flux. However, it is highly probable that we can tune one of the IRAC magnitudes, but it is difficult to think that one can tune the four at the same time. In favor of this, we note that this is not just a geometrical problem, because the flux comes from a temperature distribution that depends on the position in the wall atmosphere, which is different for different models.

In order to compare the modeled color indices with real systems, in Figure 6 the black points correspond to the Class II objects of the Hartmann et al. (2005b)'s sample of Taurus. A direct comparison shows that the objects are consistent with high inclination disks. However, a definitive answer requires a modeling of the systems one by one, which is beyond the scope of this paper.

Summarizing, the results presented in Figure 6 lead us to the conclusion that the models are not degenerate for the parameters used. In particular, if one can observationally fit the inclination (e.g., using interferometric images), a comparison of the observed and modeled colors will allow us to choose between the models.

5. SUMMARY AND CONCLUSIONS

In this paper for simplicity the heating from inner layers is not taken into account. This causes the rim to move outwards (Kama, Min, & Dominik 2009), and also changes the shape of the wall. Here, we describe the wall as a stationary well defined surface, in spite of the results of Kama et al. (2009). They developed a code that finds the sublimation wall with a detailed description of the sublimation process: the wall (dust-gas boundary) is a non-stationary diffuse region. The reason for our simplifying assumption is that the calculation of the emission for a time dependent diffuse region is a very complex issue, which depends on many unknowns. Lacking this knowledge, to pursue further the improvement of the model is not worthwhile at this moment. Our goal is to detect the differences in the SED, in particular the changes on the vertical geometry assumption, which we think will not be conspicuously modified by our assumptions.

There is a difference between the $T_{0,\mathrm{fix}}$ and $T_{0,\rho}$ walls SEDs in the wavelength range between $\lambda = 3$ and $8\,\mu$m. Due to this, the near-infrared colors calculated with a disk plus a $T_{0,\mathrm{fix}}$ wall (commonly used) and a disk plus a $T_{0,\rho}$ wall will differ. However, when analysing sets of spectra (Allen et al. 2004; Hartmann et al. 2005b) using the IRAC color-color diagrams, these differences do not change the conclusions previously presented, due to the dispersion of the models and the observations. For the modeling of spectra of real objects, the decision of which wall model is to be taken, should be done carefully.

The main conclusions are summarized next.

- A $T_{0,\mathrm{fix}}$ wall is closer than a $T_{0,\rho}$ wall. R_{wall} changes between $T_{0,\mathrm{fix}}$ or $T_{0,\rho}$ wall models, at most by 10%.

- The emission of a $T_{0,\mathrm{fix}}$ wall is larger than that of a $T_{0,\rho}$ wall.

- For each type of wall, the emission decreases as the inclination increases.

- A change in inclination is not able to match models with a $T_{0,\rho}$ and a $T_{0,\mathrm{fix}}$ wall.

- The $T_{0,\mathrm{fix}}$ wall does not show the 10 μm silicates band (see Figure 2).

- The disk for models with both types of walls shows the silicates band. For this reason, in the spectrum of the star-wall-disk system this feature is always present.

- In the IRAC color-color diagram, the $T_{0,\mathrm{fix}}$ wall models are located in a region different from that of the $T_{0,\rho}$ wall models. Between the $T_{0,\rho}$ and $T_{0,\mathrm{fix}}$ wall models, the [3.6]–[4.5] and [5.8]–[8.0] colors change by about 20% and 10%, respectively.

REFERENCES

Akeson, R. L., et al. 2005, ApJ, 635, 1173
Alibert, Y., et al. 2010, Astrobiology, 10, 19
Allen, L. E., et al. 2004, ApJS, 154, 363
Calvet, N., Magris, G., Patiño, A., & D'Alessio, P. 1992, RevMexAA, 24, 27
Calvet, N., Patiño, A., Magris, G., & D'Alessio, P. 1991, ApJ, 380, 617
Clarke, C. J., Gendrin, A., & Sotomayor, M. 2001, MNRAS, 328, 485
D'Alessio, P., Cantó, J., Calvet, N., & Lizano, S. 1998, ApJ, 500, 411
D'Alessio, P., et al. 2005, ApJ, 621, 461
Dorschner, J., Begemann, B., Henning, T., Jäger, C., & Mutschke, H. 1995, A&A, 300, 503
Draine, B. T., & Lee, H. M. 1984, ApJ, 285, 89
Dullemond, C. P., Dominik, C., & Natta, A. 2001, ApJ, 560, 957
Dullemond, C. P., & Monnier, J. D. 2010, ARA&A, 48, 205
Eisner, J. A., Graham, J. R., Akeson, R. L., & Najita, J. 2009, ApJ, 692, 309
Eisner, J. A., Hillenbrand, L. A., White, R. J., Akeson, R. L., & Sargent, A. I. 2005, ApJ, 623, 952
Eisner, J. A., Hillenbrand, L. A., White, R. J., Bloom, J. S., Akeson, R. L., & Blake, C. H. 2007, ApJ, 669, 1072
Eisner, J. A., Lane, B. F., Hillenbrand, L. A., Akeson, R. L., & Sargent, A. I. 2004, ApJ, 613, 1049
Eisner, J. A., et al. 2010, ApJ, 718, 774
Espaillat, C., et al. 2007, ApJ, 664, L111
Ferguson, J. W., et al. 2005, ApJ, 623, 585
Goldreich, P., & Ward, W. R. 1973, ApJ, 183, 1051
Gullbring, E., Hartmann, L., Briceño, C., & Calvet, N. 1998, ApJ, 492, 323
Hartmann, L., et al. 2005a, ApJ, 628, L147
Hartmann, L., et al. 2005b, ApJ, 629, 881
Hillenbrand, L. A., Strom, S. E., Vrba, F. J., & Keene, J. 1992, ApJ, 397, 613
Isella, A., & Natta, A. 2005, A&A, 438, 899
Kama, M., Min, M., & Dominik, C. 2009, A&A, 506, 1199

Mathis, J. S., Rumpl, W., & Nordsieck, K. H. 1977, ApJ, 217, 425

Mayne, N. J., & Harries, T. J. 2010, MNRAS, 409, 1307

McClure, M., et al. 2010, ApJS, 188, 75

Millan-Gabet, R., Malbet, F., Akeson, R., Leinert, C., Monnier, J., & Waters, R. 2007, in Protostars and Planets V, ed. B. Reipurth, D. Jewitt, & K. Keil (Tucson: Univ. Arizona Press), 539

Monnier, J. D., et al. 2005, ApJ, 624, 832

Nagel, E., D'Alessio, P., Calvet, N., Espaillat, C., Sargent, B., Hernández, J., & Forrest, W. J. 2010, ApJ, 708, 38

Pollack, J. B., Hollenbach, D., Beckwith, S., Simonelli, D. P., Roush, T., & Fong, W. 1994, ApJ, 421, 615

Quillen, A. C., Blackman, E. G., Frank, A., & Varnière, P. 2004, ApJ, 612, L137

Sipos, N., et al. 2009, A&A, 507, 881

Suzuki, T. K., Muto, T., & Inutsuka, S.-I. 2010, ApJ, 718, 1289

Tannirkulam, A., Harries, T. J., & Monnier, J. D. 2007, ApJ, 661, 374

Tannirkulam, A., et al. 2008, ApJ, 677, L51

Tuthill, P. G., Monnier, J. D., & Danchi, W. C. 2001, Nature, 409, 1012

Verhoelst, T., et al. 2006, A&A, 447, 311

Whitney, B. A., Indebetouw, R., Bjorkman, J. E., & Wood, K. 2004, ApJ, 617, 1177

Nuria Calvet: Department of Astronomy, University of Michigan, Ann Arbor, MI, 48109, USA (ncalvet@umich.edu).

Paola D'Alessio: Centro de Radioastronomía y Astrofísica, Universidad Nacional Autónoma de México, Apdo. Postal 3-72, 58090 Morelia, Michoacán, Mexico (p.dalessio@crya.unam.mx).

Catherine Espaillat: Harvard-Smithsonian Center for Astrophysics, Cambridge, MA, 02138, USA (cespaillat@cfa.harvard.edu).

Erick Nagel and Miguel Angel Trinidad: Departamento de Astronomía, Universidad de Guanajuato, 36240, Guanajuato, Guanajuato, Mexico (erick, trinidad@astro.ugto.mx).